Tunable magnetic order in transition metal doped, layered, and anisotropic Bi_2O_2Se: Competition between exchange interaction mechanisms

Xiaopeng Liu,[1] Dominik Legut,[2] Ruifeng Zhang,[1] Tianshuai Wang,[1] Yanchen Fan,[1] and Qianfan Zhang[1,*]
[1]*School of Materials Science and Engineering, Beihang University, Beijing 100191, P. R. China*
[2]*IT4Innovations, VSB-Technical University of Ostrava, 17.listopadu 2172/15, CZ-70800 Ostrava-Poruba, Czech Republic*

(Received 13 May 2019; published 26 August 2019)

Bi_2O_2Se is a novel layer-structured material with high electron mobility, while its efficiency could be greatly improved by doping different elements to introduce a magnetic spin order. We investigated the electronic and magnetic properties of various transition metal (TM) (TM = Mn, Cr, Fe, Co, and Ni) doped Bi_2O_2Se within a framework of density functional theory (DFT), and discovered that $Bi_{2-n}X_nO_2Se$ exhibits long-range magnetic ordered structure via competition among double-exchange, *p-d* exchange, and superexchange interaction. The magnetic order of the bulk phase in which the magnetic atoms form interlayer coupling would vary with the type and concentration of doped atoms, but all the layered phases in which the magnetic atoms are in-plane coupled show ferromagnetic order. By combing DFT calculations with the Monte Carlo scheme, we solve the exchange interaction constants for the Heisenberg model and further evaluate the Curie temperatures of $Bi_{2-n}X_nO_2Se$. Ferromagnetic order for most doped systems exhibit to be robust with high Curie temperature, some of which overcomes room temperature (for 12.5% Co-doped layer Bi_2O_2Se). It is also worth mentioning that the appearance of impurity energy levels narrows the band gap and enhances the spin-orbit coupling of *d* orbitals and therefore increase large magnetic anisotropy energy. Our study demonstrates a potential pathway to design new dilute magnetic semiconductors through doping of $Bi_{2-n}X_nO_2Se$ by magnetic transitional elements.

DOI: 10.1103/PhysRevB.100.054438

I. INTRODUCTION

Due to the increasing demand for electronic components with high information transmission efficiency and low energy consumption, dilute magnetic semiconductors (DMSs) [1], which can exploit not only the charge properties but also the spin of carriers, has become more valuable. Furthermore, the field effect devices can be constructed for the intrinsic two-dimensional (2D) semiconductors due to the electrostatic shielding in the original block weakened, thus, 2D DMS has become a new focus in this field. The strategy on doping transition metal (TM) impurities (Cr, Mn, Fe, Co, Ni) into 2D semiconductors [2], which can induce the long-range order, becomes one of the most important schemes to achieve the ferromagnetic semiconducting device. Since high mobility magnetic thin film semiconductors can lead to scalable fabrication of high performance devices, numerous works have focused on 2D DMS with high mobility [3–5]. In previous works, a large magnetic moment, suitable semiconductor band gap, and high Curie temperature (T_c) became primary goals of the research. Meanwhile, two-dimensional magnetic anisotropy is also a significant factor. Because the strong thermal fluctuations may easily destroy the 2D ferromagnetism according to the Mermin-Wagner theorem, the presence of a spin-wave excitation gap which is a direct result of magnetic anisotropy with out-of-plane easy axis is essential for long-range ferromagnetic order in the layer phase at finite (nonzero) temperatures [3,6]. To achieve attractive properties, both the pristine semiconductor and the doping element are critical for its realistic application. In our paper we explore the 2D DMS species by magnetic transitional metal doping with the emphasis of the electrostatic interlayer forces.

Recently, the layer-structured material Bi_2O_2Se with electrostatic interaction as the interlayer force, which possesses extremely high electronic mobility, attracted great interest [7–9] and has already been demonstrated to be the promising semiconductor as the top-gated field-effect transistors and pyroelectric material. The excellent properties of Bi_2O_2Se inspire people to explore its application as the magnetic semiconductor. First, the Bi-O or Bi-Se based compounds have been demonstrated to exhibit strong exchange coupling when doped by the magnetic element, and hence the stable ferromagnetic order can be expected in Bi_2O_2Se. Second, the heavy element Bi and the crystal field splitting of TMs cause the hybridization of TMs and O increasing the strong spin-orbit interaction and leading to stronger magnetic anisotropy energy (MAE). Third, the layered-structure nature of Bi_2O_2Se provides the opportunity for the preparation of magnetic layered-structure materials, which is also one of the most important topics in the field of low-dimensional materials [7–9] and therefore deserves a following detailed study.

In the present work we theoretically explore the effect of TMs doping in both bulk and monolayered Bi_2O_2Se phases, and investigated different ferromagnetic properties under different doping elements and various doping levels. On the basis of the charge distribution analysis and bonding conditions of the stable structure, we explain the formation of the long-range magnetic order from the point of exchange interactions. Our Monte Carlo simulation along with the exchange

*Corresponding author: qianfan@buaa.edu.cn

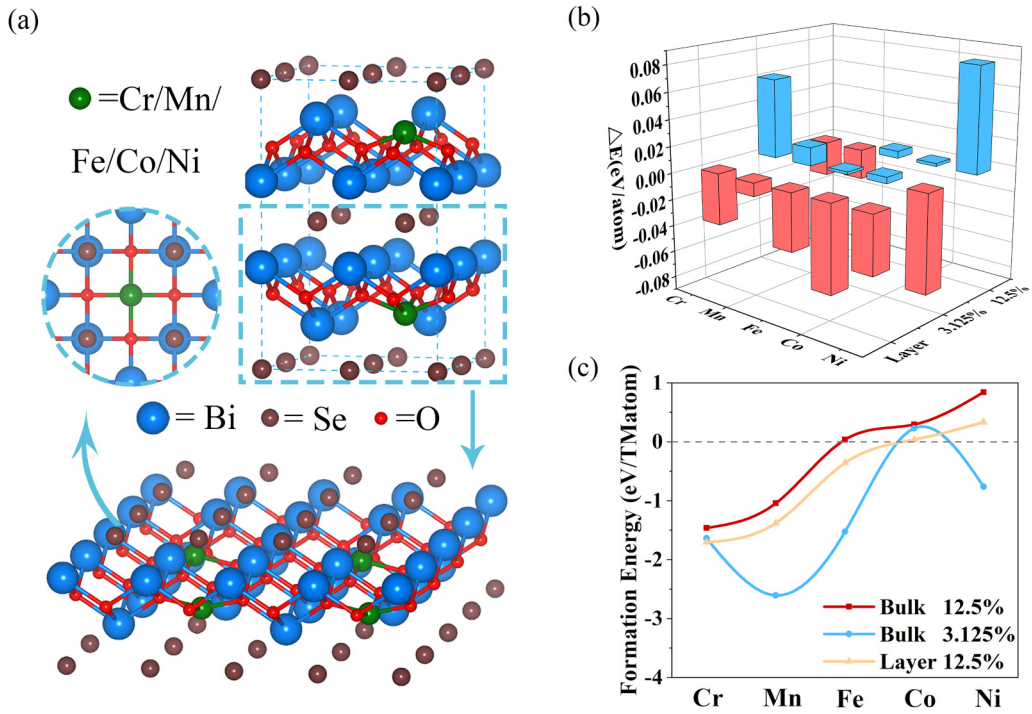

FIG. 1. (a) Crystal structures of TMs-doped $Bi_{2-n}X_nO_2Se$. (b) ΔE_{FM-AFM} of $Bi_{2-n}X_nO_2Se$ in different doping phases. In layer phases, all dopants are FM; in 12.5% bulk phases, Cr and Mn dopant are FM; and in 3.125% bulk phases, Ni dopant are FM. (c) Upper limit of average formation energy (E_f/N_{TM}) of TM doping Bi_2O_2Se.

parameters based on the Heisenberg model and electronic structure are presented, showing a clear trend on the formation of ferromagnetic phase and the stability of long-range order even near the room temperature [10]. Furthermore, it is found that the strong spin-orbit coupling induces a strong magnetic anisotropic effect similar to the one in Ref. [11]. From bulk phase to layer phase, the anisotropic energy is significantly enhanced, which proved that most of the TMs-doped layered phases have two-dimensional ferromagnetic order. The only exception is for the Fe-doped layered phase. Based on the spin-orbit coupling matrix elements, we can analyze the source of magnetic anisotropy. To conclude, this work has discovered TM-doping 2D layered ferromagnetic semiconductors with high Curie temperature and magnetic anisotropy, and the generation of magnetic sequence is analyzed, which will further broaden the horizon for the development of the DMSs.

II. METHODOLOGY

All the first-principles calculations are performed using the Vienna *ab initio* simulation package (VASP). Electron exchange and correlation effects are treated by Perdew-Burke-Ernzerhof (PBE) parametrized generalized gradient approximations [12]. Kinetic energy cutoff for the plane waves is set at 500 eV; sampling of the Brillouin zone for bulk of $2 \times 2 \times 1$ and $4 \times 4 \times 1$ supercells are done with $9 \times 9 \times 9$ and $6 \times 6 \times 8$ k-points meshes, while for the layer sample with k-points meshes $11 \times 11 \times 1$ and $9 \times 9 \times 1$ k points. When calculating the MAE we increased a set k-points mesh to a $10 \times 10 \times 1$ grid to ensure the accuracy of total energy. To optimize conformations of the doped system, fully structure relaxation is performed until the forces become lower than 0.01 eV/A. For the correction of the on-site repulsive interaction, the transition element d electron states atoms are treated by the LDA+U method introduced by Dudarev [13], and $U - J = 5$ eV was used in order to increasing Coulomb repulsive potential. The value of $U - J$ was obtained by fitting the results calculated by HSE06 [14], as shown in Sec. II of the Supplemental Material [15]. In order to study the relationship between the magnetic properties and the doping concentration, we have designed both bulk (12.5%, 3.125%) and layer (12.5%) different doping levels. As shown in Fig. 1(a), we selected Cr, Mn, Fe, Co, and Ni as the magnetic doping elements. They are the commonly used dopants for introducing the magnetic moment, and we will also show their strong spin polarization in the following text. Here we focused on the study of the band structure, the long-range magnetic order, the T_c, and the magnetic anisotropic effect, which are also the main concerns in the field of magnetism.

III. RESULTS AND DISCUSSION

A. Magnetic order and density of states analysis

Doping TM atoms into semiconductors, the magnetic ground state depends on the coupling state of the impurity atom and its surrounding atoms, and spin polarized state for TM dopants can be formed. As one kind of layered structure material, the magnetic properties of layered $Bi_{2-n}X_nO_2Se$ is very important, and it can be predicted that the electronic structure and magnetic order should be also quite different. Before investigating the electronic and magnetic properties, we first survey the upper (rich-Bi) and lower limits

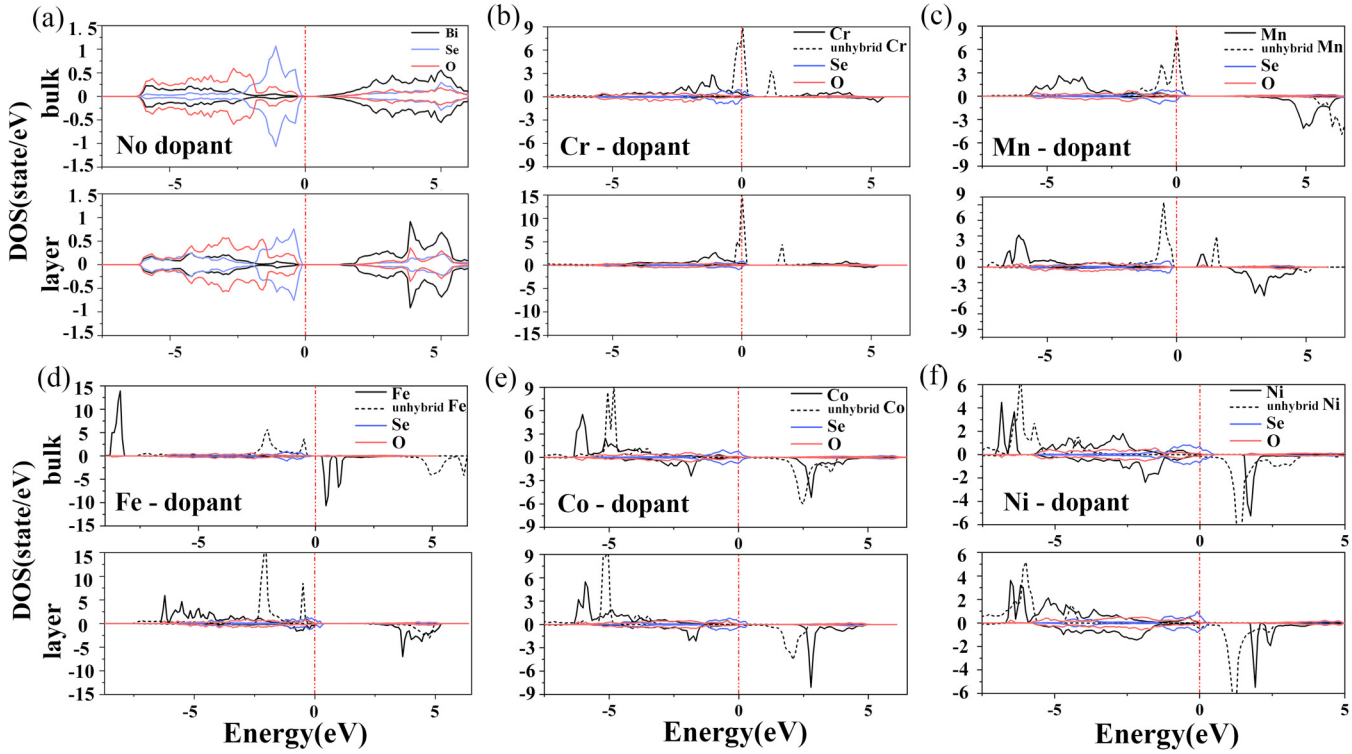

FIG. 2. The spin-resolved projected density of states of the *d* orbit of TM (TM = Cr, Mn, Fe, Co, Ni) and unhybrid TM, *p* orbit of Se and O. Bulks and layers with 12.5% dopant are above and down, respectively. The Fermi level is denoted by a dashed line at 0 eV.

(poor-Bi) of formation energy, as summarized in Sec. I of the Supplemental Material [15–17]. Obviously all TM doped phases in the Bi-poor environment are more stable than in the rich-Bi environment. It can be seen that most phases are thermodynamically stable. Although Co/Ni-doped 12.5% bulk phase, Co-doped 3.125% bulk phase, and Ni-doped layer phase [as shown in Fig. 1(c)] are thermodynamically unstable in the rich-Bi case, the synthesis of those phases would be facile in the poor-Bi case. Oxygen plays an important role in the formation of long-range order as it acts as a bridge for coupling. Here we simulated the doping effect of magnetic elements both in a monolayer as well as in bulk Bi_2O_2Se. Based on the fact that all of the dopants possess the overall spin polarization, we discussed the long-range magnetic order, and see whether the spin polarization prefers to stay ferromagnetic (FM) or antiferromagnetic (AFM). Here the parameter $\Delta E_{\text{FM-AFM}}$, which is defined as the energy difference between AFM order and FM order, is calculated to identify the stable magnetic order (positive value means FM state is energetically favored, while negative value stands for more stable AFM state).

The long-range magnetic orders and the magnitudes of $\Delta E_{\text{FM-AFM}}$ for both layered and bulked phases (with both the doping concentrations of 12.5% and 3.125%) are summarized in Fig. 1(b). The layered phase exhibits quite different magnetic stability compared to the bulk phase. In general, the layered phase exhibits much higher $\Delta E_{\text{FM-AFM}}$ and FM order is energetically more favored. In bulk phases, both FM and AFM orders can be formed for different kinds of dopants. In the 12.5% doping level of bulk phase, $Bi_{1.75}Cr_{0.25}O_2Se$ and $Bi_{1.75}Mn_{0.25}O_2Se$ prefer the FM order. In the 3.125% doping level of bulk phase, only $Bi_{1.9375}Ni_{0.0625}O_2Se$ exhibits FM order. These sentences imply that the others are AFM ordering. The magnetism of DMSs comes from the on-site electrons of the TM atoms, and as the *d* electrons of TM atoms occupy different orbits, the energy and magnetism changes. The doped atoms cause the rearrangement of electrons among neighboring atoms, which make a great influence on the edge state of $Bi_{2-n}X_nO_2Se$. In order to investigate the coupling between TMs and surrounding atoms, we calculated the density of state (DOS) for Cr-, Mn-, Fe-, Co-, and Ni-doped $Bi_{2-n}X_nO_2Se$, as shown in Figs. 2(a)–2(f).

The magnetic order is determined by the competition between different magnetic exchange mechanisms, which is the fundamental origination of the different magnetic order induced by various concentrations or distances between TM elements. These mechanisms are as follows: (1) States broadening near the highest occupied molecular orbital (double exchange interaction). (2) Coupling of *p* orbitals of Se and *d* orbitals of TMs (*p*-*d* exchange interaction). (3) Indirect exchange through the electron cloud of intermediate atoms (superexchange interaction) [1]. In the bulk phase with 12.5% doping level, it can be seen from Figs. 2(b) and 2(c) that Cr/Mn doping elements bring states to the valence bands in a way the system becomes metallic [18]. Such a dispersive band is induced by the strong hybridization between *d* orbits of TMs and *p* orbits of Se, while the states of *d* orbits were broadened and new antibonding orbits were formed, see Fig. 3. Such characteristics of hybridization clearly indicate the double exchange interaction [10,19]. Meanwhile, the *p*

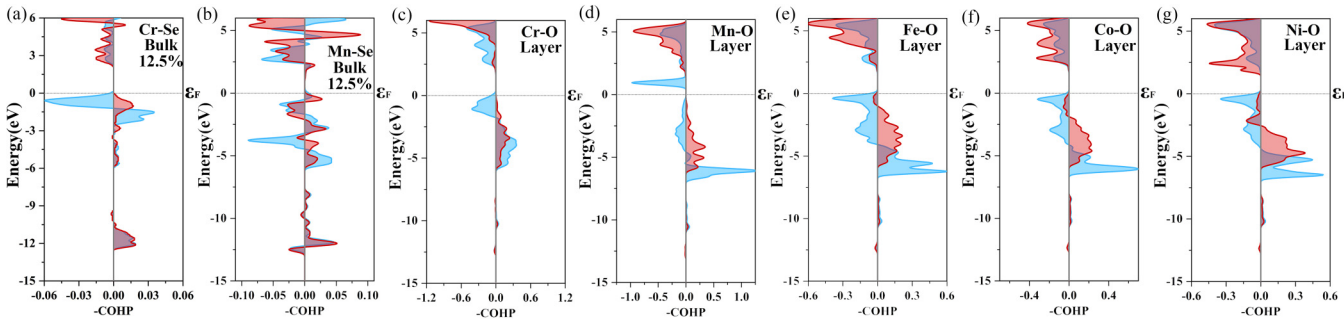

FIG. 3. Crystal orbital Hamiltonian population analysis of spin polarization and chemical bonding in FM order phase. The blue and red region indicates that the spin is up and down, respectively. If −COHP <0 (>0), two atoms hybridize in this energy region to form an antibonding orbital (bonding orbital). State of TM-O/Se is a generally bonding state in low energy level, and the antibonding orbitals are partially occupied. (a) and (b) COHP of Cr/Mn-Se in bulk 12.5% phases. (c)–(g) COHP of Cr/Mn/Fe/Co/Ni-O in layer 12.5% phases, respectively.

orbits of Se are hybridized with the *d* orbits of TM, causing the *p* orbit of Se splits. The state of upward spin moves to the region of the high energy, and the state of downward spin is basically fully filled, which induces magnetic moment on Se. The magnetic moment is arranged antiparallel to the TM magnetic moment [20]. With the induced magnetic moment of Se as a bridge, TM atoms can form long-range ferromagnetic coupling. Also, there is an antiferromagnetic superexchange between TM-Se-TM which competes with the *p-d* exchange [21]. When two atoms are antiferromagnetic coupled by the superexchange, the fully occupied states at the low energy level are shifted to the lower energy region and the unoccupied states at the high energy level move to even higher energy region, thus band energy is gained which stabilizes the antiferromagnetic coupling. Through crystal orbital Hamiltonian population analysis (COHP) [18,22,23], as shown in Figs. 3(a) and 3(b), we find that the antibonding orbitals formed by Cr/Mn and Se atoms are partially occupied and close to the highest occupied state. Because the *d* orbitals of the two TMs are less than half-filled, their superexchange interaction is also weakened, which makes them gain energy by ferromagnetic order formation. On the contrary, in the case of Fe, Co, and Ni dopants, as shown in Figs. 2(d)–2(f), the PDOS profile shows a highly localized state far from Fermi level, which becomes dispersive after the hybridization between impurity elements and Se atoms. This strong antiferromagnetic exchange leads to the appearance of antiferromagnetic order.

As for bulk phase with 3.125% doping level, only $Bi_{1.9375}Ni_{0.0625}O_2Se$ shows FM order while others are AFM order. With the decrease of the doping concentration of TM atoms, the distance of the nearest neighbor TM atoms becomes a little shorter, but the distance of the next nearest neighbor TM atom is large enough to ignore the interaction between these two atoms, causing the broadening of the states near Fermi level of $Bi_{1.9375}X_{0.0625}O_2Se$ which decrease compared to the bulk $Bi_{1.75}X_{0.25}O_2Se$ (X = Cr, Mn). Superexchange effect still stays strong and therefore such a doped system exhibits an antiferromagnetic ordering. For $Bi_{1.9375}Ni_{0.0625}O_2Se$, the *d* orbitals of Ni strongly hybridized with the *p* orbitals of Se and O atoms, resulting in full band shift to lower energies, and the stronger *p-d* coupling and exchange effects make the FM order preferable.

For the monolayered phases, all of the dopants induce the FM order. As a short-range exchange interaction, superexchange interaction is greatly weakened in the layered phase resulting from the coupling and transfer of electrons in different orbitals within just limited two dimensions. It can be seen from Figs. 2(a)–2(f) that the TM atoms have strong bonding with the surrounding O atoms. Because the 2D quantum effect is more significant in the layered system, the contribution by the indirect exchange interaction will dominate these layered systems [24,25]. Through COHP analysis illustrated in Figs. 3(c)–3(g), the bonding of TM and O in the layered phase is highly consistent: the orbits in the valence band are all antibond orbitals, and the antibond orbitals in the conduction band are partially occupied, which ensures the stability of the ferromagnetic order.

B. Magnetic exchange interaction and Curie temperature

T_c is one of the most important physical quantities to evaluate the properties of DMSs, especially for the stability of ferromagnetic order. Here we chose the Monte Carlo (MC) model [26] to evaluate the T_c. For most magnetic materials, the exchange interactions are the dominant contribution to the ordered arrangement of atomic magnetic moments, and the exchange interaction strength J_{ij} is the most important parameter to describe the interactions between spins S_i and S_j by the equation

$$\boldsymbol{H}_{\rm ex} = -\sum_{i,j} \boldsymbol{J}_{ij}\boldsymbol{S}_i\boldsymbol{S}_j, \tag{1}$$

in which $H_{\rm ex}$ is Heisenberg model Hamiltonian.

We need to construct different antiferromagnetic and subferromagnetic structures to solve this set of linear equations to obtain the J_{ij} values. By ignoring the negligible interaction between the farthest magnetic atoms, we evaluate exchange interaction by constructing the first-, second-, and third-neighbor exchange coupling parameters J_1, J_2, and J_3 [27,28]. These parameters can be achieved by computing the total energies per formula unit for four kinds of long-range orders: the ferromagnetic order (E_0), the type I antiferromagnetic order (E_1), the type II antiferromagnetic order (E_2), and type III antiferromagnetic (E_3) order (magnetic orders of the layer

TABLE I. Electrons in each d orbital, magnetic moment of each doping TM, exchange constants J_1, J_2, and J_3 calculated by Eqs. (2)–(5).

Electrons	d_{xy}	d_{yz}	d_{z^2}	d_{xz}	$d_{x^2-y^2}$	Magn. moment/μB	J_1/meV	J_2/meV	J_3/meV
Cr↑	0.96	0.92	0.93	0.91	0.23	3.81	5.04	2.73	2.34
Cr↓	−0.01	−0.03	−0.02	−0.07	−0.14				
Mn↑	0.94	0.95	0.94	0.95	0.96	4.65	9.41	1.58	2.57
Mn↓	−0.11	−0.07	−0.01	−0.01	−0.01				
Fe↑	0.98	0.98	0.97	0.98	0.99	4.18	AFM	AFM	AFM
Fe↓	−0.07	−0.17	−0.11	−0.18	−0.31				
Co↑	0.97	0.97	0.96	0.97	0.99	2.74	AFM	AFM	AFM
Co↓	−0.95	−0.05	−0.95	−0.05	−0.15				
Ni↑	0.98	0.97	0.96	0.97	0.99	1.63	AFM	AFM	AFM
Ni↓	−0.07	−0.96	−0.94	−0.96	−0.35				
Layer Cr↑	0.95	0.91	0.91	0.94	0.25	3.81	14.13	11.61	6.22
Layer Cr↓	−0.03	−0.03	−0.03	−0.03	−0.16				
Layer Mn↑	0.96	0.95	0.93	0.95	0.54	3.95	10.42	3.95	1.54
Layer Mn↓	−0.06	−0.05	−0.06	−0.04	−0.25				
Layer Fe↑	0.97	0.97	0.95	0.97	0.99	3.74	12.52	10.82	7.21
Layer Fe↓	−0.03	−0.03	−0.91	0.03	0.17				
Layer Co↑	0.97	0.97	0.95	0.97	0.99	2.73	10.23	27.84	7.41
Layer Co↓	−0.95	−0.06	−0.94	−0.05	−0.17				
Layer Ni↑	0.98	0.98	0.96	0.97	0.99	1.69	12.93	6.32	4.01
Layer Ni↓	−0.97	−0.08	−0.92	−0.96	−0.31				

phase are illustrated by Fig. S2 in the Supplemental Material [15]).

For bulk phase, the relationship between the calculated energies and the exchange parameters can be expressed as

$$\boldsymbol{E}_0 = \boldsymbol{E} - \boldsymbol{S}^2(4\boldsymbol{J}_1 + 8\boldsymbol{J}_2 + 8\boldsymbol{J}_3), \tag{2}$$

$$\boldsymbol{E}_1 = \boldsymbol{E} - \boldsymbol{S}^2(4\boldsymbol{J}_1 - 8\boldsymbol{J}_2 - 8\boldsymbol{J}_3), \tag{3}$$

$$\boldsymbol{E}_2 = \boldsymbol{E} - \boldsymbol{S}^2(-4\boldsymbol{J}_1 - 8\boldsymbol{J}_2 + 8\boldsymbol{J}_3), \tag{4}$$

$$\boldsymbol{E}_3 = \boldsymbol{E} - \boldsymbol{S}^2(-4\boldsymbol{J}_1 + 8\boldsymbol{J}_2 - 8\boldsymbol{J}_3). \tag{5}$$

Then the J_1,J_2, and J_3 can be solved as

$$\boldsymbol{J}_1 = -\frac{\boldsymbol{E}_0 + \boldsymbol{E}_1 - \boldsymbol{E}_2 - \boldsymbol{E}_3}{16\boldsymbol{S}^2}, \tag{6}$$

$$\boldsymbol{J}_2 = -\frac{\boldsymbol{E}_0 - \boldsymbol{E}_1 - \boldsymbol{E}_2 + \boldsymbol{E}_3}{32\boldsymbol{S}^2}, \tag{7}$$

$$\boldsymbol{J}_3 = -\frac{\boldsymbol{E}_0 - \boldsymbol{E}_1 + \boldsymbol{E}_2 - \boldsymbol{E}_3}{32\boldsymbol{S}^2}. \tag{8}$$

For layer phases, the relationship between the calculated energies and the exchange parameters can be expressed as

$$\boldsymbol{E}_0 = \boldsymbol{E} - \boldsymbol{S}^2(4\boldsymbol{J}_1 + 8\boldsymbol{J}_2 + 2\boldsymbol{J}_3), \tag{9}$$

$$\boldsymbol{E}_1 = \boldsymbol{E} - \boldsymbol{S}^2(4\boldsymbol{J}_1 - 8\boldsymbol{J}_2 - 2\boldsymbol{J}_3), \tag{10}$$

$$\boldsymbol{E}_2 = \boldsymbol{E} - \boldsymbol{S}^2(2\boldsymbol{J}_3), \tag{11}$$

$$\boldsymbol{E}_3 = \boldsymbol{E} - \boldsymbol{S}^2(-4\boldsymbol{J}_1 + 8\boldsymbol{J}_2 - 2\boldsymbol{J}_3). \tag{12}$$

Then the J_1,J_2, and J_3 can be solved as

$$\boldsymbol{J}_1 = -\frac{2\boldsymbol{E}_0 + \boldsymbol{E}_1 - 2\boldsymbol{E}_2 - \boldsymbol{E}_3}{16\boldsymbol{S}^2}, \tag{13}$$

$$\boldsymbol{J}_2 = -\frac{2\boldsymbol{E}_0 - \boldsymbol{E}_1 - 2\boldsymbol{E}_2 + \boldsymbol{E}_3}{32\boldsymbol{S}^2}, \tag{14}$$

$$\boldsymbol{J}_3 = -\frac{-\boldsymbol{E}_1 + 2\boldsymbol{E}_2 - \boldsymbol{E}_3}{8\boldsymbol{S}^2}. \tag{15}$$

After the exchange correlation coefficient is obtained (Table I) [29], the MC simulation can be carried out, and the T_c can be achieving by fitting the function:

$$\boldsymbol{m}(\boldsymbol{T}) = \boldsymbol{\alpha}\left(1 - \frac{\boldsymbol{T}}{\boldsymbol{T}_c}\right)^{\beta}, \tag{16}$$

when $m(T)$ approaches 0.

The T_c can be accurately extracted from characteristic temperature for the materials as illustrated in Fig. 4. Different dopants can result in quite different T_c, and we note that the T_c obviously exceed the liquid nitrogen temperature (77 K) [30]. In the system of bulk, both $Bi_{1.75}Cr_{0.25}O_2Se$ and $Bi_{1.75}Mn_{0.25}O_2Se$ exhibit the T_c between 104 and 138 K [Fig. 4(b)]. For $Bi_{1.9375}Ni_{0.0625}O_2Se$, the magnitude of T_c is as high as 199 K, which can be viewed as the material with very good magnetic stability, even comparing with the commonly used ferromagnetic materials [31,32]. The value of T_c primarily determined by the strength of J_{ij}, and the stronger magnetic coupling correlation, can always induce the more stable magnetic order against the thermal fluctuations.

It can be also predicted that different T_c can be induced by the monolayered doped phases. In Fig. S5(c) the magnetization evolutions for different dopants are plotted [15]. The magnitudes of T_c for Cr, Fe, Co, and Ni dopants can be as high as 210, 151, 317, and 132 K, respectively. Therefore, the layered phase not only provides more choices on realizing the

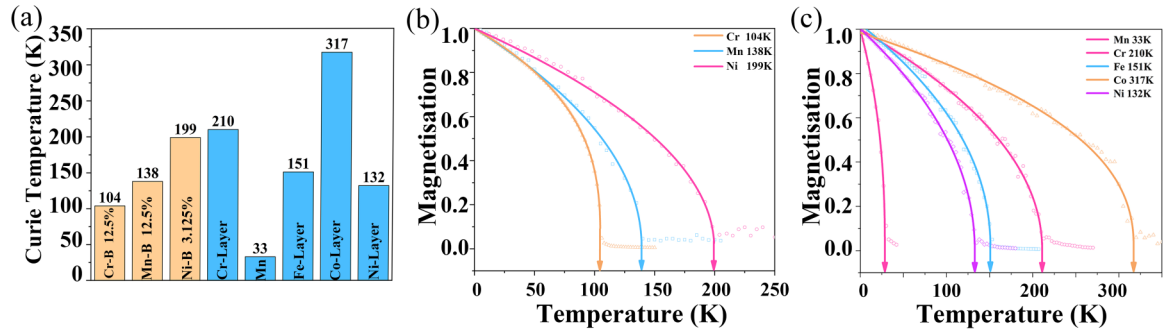

FIG. 4. (a) Curie temperature of bulk and layer $Bi_{2-n}X_nO_2Se$. (b) Monte Carlo simulation curves and T_c of bulk phases: $Bi_{1.75}Mn_{0.25}O_2Se$ (104 K), $Bi_{1.75}Cr_{0.25}O_2Se$ (138 K), and $Bi_{1.9375}Ni_{0.0625}O_2Se$ (199 K). (c) Monte Carlo simulation curves and T_c of layer phases. Cr dopant (210 K), Mn dopant (33 K), Fe dopant (151 K), Co dopant (317 K), and Ni dopant (132 K).

FM order, but also induces very robust magnetization, even at room temperature, i.e., for Co dopant. This can be understood by the existence of the interlayer interactions only in monolayered $Bi_{2-n}X_nO_2Se$, as the intralayer coupling disappears. Such high T_c is mainly attributed to the larger value of J_{ij} within the $x-y$ plane of the layered phase, which depends on the strength of Ruderman-Kittel-Kasuya-Yosida exchange under different correlative paths. As can be seen from Table I, there is little difference among the value of parameter J_1, so the indirect exchange J_2 and J_3 are the determining factors of T_c. The simulation result clearly indicates that the high T_c can be achieved by magnetic element doping, and such ferromagnetic $Bi_{2-n}X_nO_2Se$ can be even possibly applied in the manufacture of electronic components.

C. Band structure and electron occupation

We further discuss the band structure and electron occupation of $Bi_{2-n}X_nO_2Se$. Compared with the freestanding transition metal atoms, the electronic arrangement of the doped atoms in diluted magnetic semiconductors has changed significantly because of the strong electronegativity of O atoms around the TM atoms. In Table I we listed the integrated occupation number for five d orbit components for both up-spin and down-spin electrons. A remarkable rearrangement of electrons occurs due to the crystal field of transition metal atoms. It can be clearly seen that the up-spin state is always fully occupied (occupation number approaches one) except for Cr dopant, and the number of occupied down-spin states then determines the overall magnetic moment. That is the reason why the Mn atom, which possesses the half-filled configuration, can induce the largest spin polarization among all of the dopants.

We further studied the spatial spin distribution in order to achieve the interaction mechanism between TM and the surrounding anions. The spin charge density is quantitatively analyzed and plotted in Fig. S6 [15]. It is strongly indicated that the neighboring ions are also spin polarized due to the exchange effect, especially O atoms. As shown in Figs. S6(a) and S6(b), the coupling between Cr/Mn dopants and O/Se is antiferromagnetic [15]. In terms of electron occupation, the orbits in the z direction of Cr and Mn are always in a semifull state, and the Cr/Mn states are generally close to the highest occupied state. Such an arrangement of electrons results [Figs. 2(b) and 2(c)] in the splitting between the up and down symmetric energy levels of Se and the shift of the upward spin energy levels to the higher energy. Following with such asymmetry of the filling of Se electrons, the p-d exchange interaction is very significant [29].

The band structures for 3.125% doped bulk, 12.5% doped bulk, and 12.5% doped monolayered phases are shown as Figs. S3 and S2 in the Supplemental Material [15] and Fig. 5, respectively. As the indirect band gap semiconductor, the composition of conduction band minimum (CBM) and valance band maximum (VBM) of Bi_2O_2Se, respectively, are dominated by the hybridization between p_x, p_y orbits of Se atoms and p_z orbits of Bi atoms [33]. When doping with the TM atoms into Bi_2O_2Se, impurity energy levels are introduced into the band structure. It is obvious that the flat bands with weak dispersions are contributed by the delocalized d orbitals. Energy bands of 12.5% Cr-/Ni-doped layer and 12.5% Cr-/Mn-/Ni-doped bulk are similar to a metal case: their highest occupied states (Fermi levels) are in valence band. We also notice that the dopants in bulk cases except Co and in layered ones except Ni can change the band gap from the indirect one into the direct one with both VBM and CBM located at the Γ point. Due to the increase of electrons by the doped atoms, semiconductors exhibit the characteristics of N type.

The d orbits of different transition metal atoms are introduced into the band gap, which makes it easier for electrons to transfer into higher energy levels [34]. In all energy bands, the states close to the highest occupied state are always composed of the p orbitals of the Se atom. After doping, TMs hybridize with adjacent Se atoms, and the resulting states appear at the vicinity of the highest occupied state and at the band gap. In the bulk materials doped with Fe, Co, or Ni atoms, some of the mixed state locates within the band gap, while doped with Cr/Mn, these states tend to appear at the band edge. In contrast, in the layered phases, the mixed state is always located in the band gap. Due to the quantum confinement effect, the band gap of layered phase is broadened, which makes it possible to modulate the properties of semiconductors. To summarize, the hybridization of the d orbits of the TMs and p orbits of the neighbor atoms results in a band energy change and the electrons distribution. This

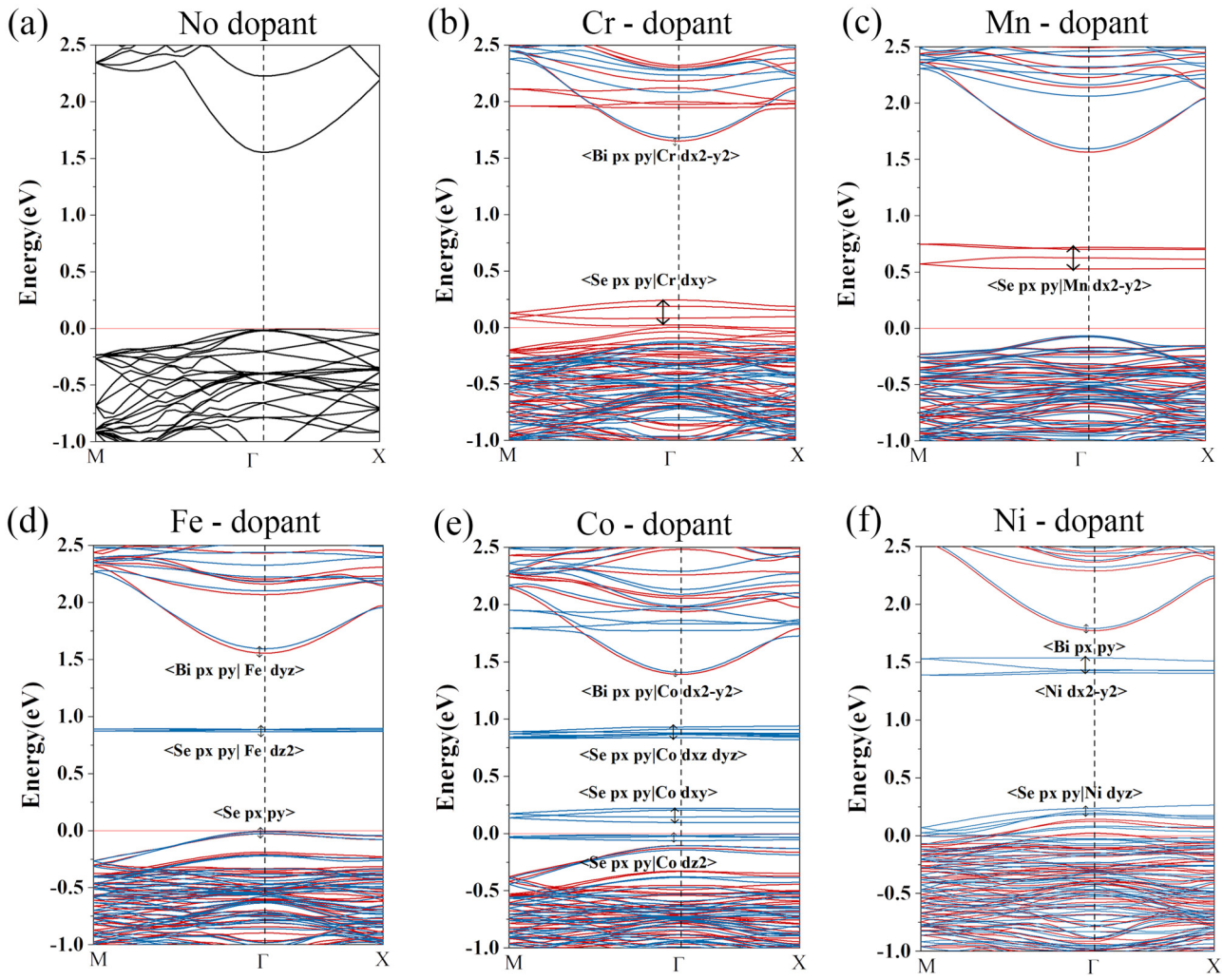

FIG. 5. (a)–(f) Band structure of TMs doped layer $Bi_{2-n}X_nO_2Se$ (12.5% doping level). The band gaps of DMSs are 1.56, 0.53, 1.48, 0.89, 0.17, and 1.34 eV, respectively. Red and blue lines are spin-up (majority spin) and spin-down (minority spin) band, respectively. The impurity states in the forbidden band are generally formed by the hybridization of the *p* orbitals of Se and the partial *d* orbitals of TMs.

induces the exchange splitting for up and down electrons (a generation of a net spin magnetic moment). At the same time, it improves the original semiconductor properties through reducing band gap and making the electronic transition easier.

D. Magnetic anisotropy energy

The magnetic energy (crystalline) anisotropy, which corresponds to the magnetization orientation dependent properties of the FM system, is one of the most important magnetic properties for spintronic applications. The orientation of spin polarization corresponds to the minimum of the total energy along magnetization direction (easy axis) at low temperature. We evaluate the magnetic anisotropic energy (MAE) by calculating the difference of total energies on magnetization directions of [001] and [100] ($\mathbf{MAE} = \boldsymbol{E}_{[001]} - \boldsymbol{E}_{[100]}$) including the spin-orbit coupling (SOC). According to this definition, positive MAE stands for the in-plane magnetic anisotropy, while negative MAE stands for the perpendicular magnetic anisotropy. According to the previous description, the existence of two-dimensional layered magnetic order is based on large magnetic anisotropy with easy axis along [001] direction. We mainly consider the monolayered phase and demonstrate that the magnetic anisotropy of Bi_2O_2Se-based diluted magnetic semiconductors is increased by doped magnetic atoms significantly.

The magnitudes of MAE for five doped elements are shown as Fig. 6(a). In general, layered $Bi_{2-n}X_nO_2Se$ exhibits remarkable MAE. Cr-, Mn-, Co-, and Ni-doped systems tends to prefer the [001] magnetization axis by 1.10, 0.46, 0.46, and 1.04 meV/TM atom, respectively. In contrast, an Fe-doped system exhibit in-plane magnetic anisotropy, as large as 2.75 meV/TM atom. The strength of magnetic anisotropy in doped Bi_2O_2Se with FM order is comparable or even larger than that in other 2D intrinsic or doped ferromagnetic material [4,30,35]. Compared with bulk phases, the MAE of layered phases is one order of magnitude higher.

In order to explore the origin of magnetic anisotropy, we construct *k*-resolved anisotropy by means of force

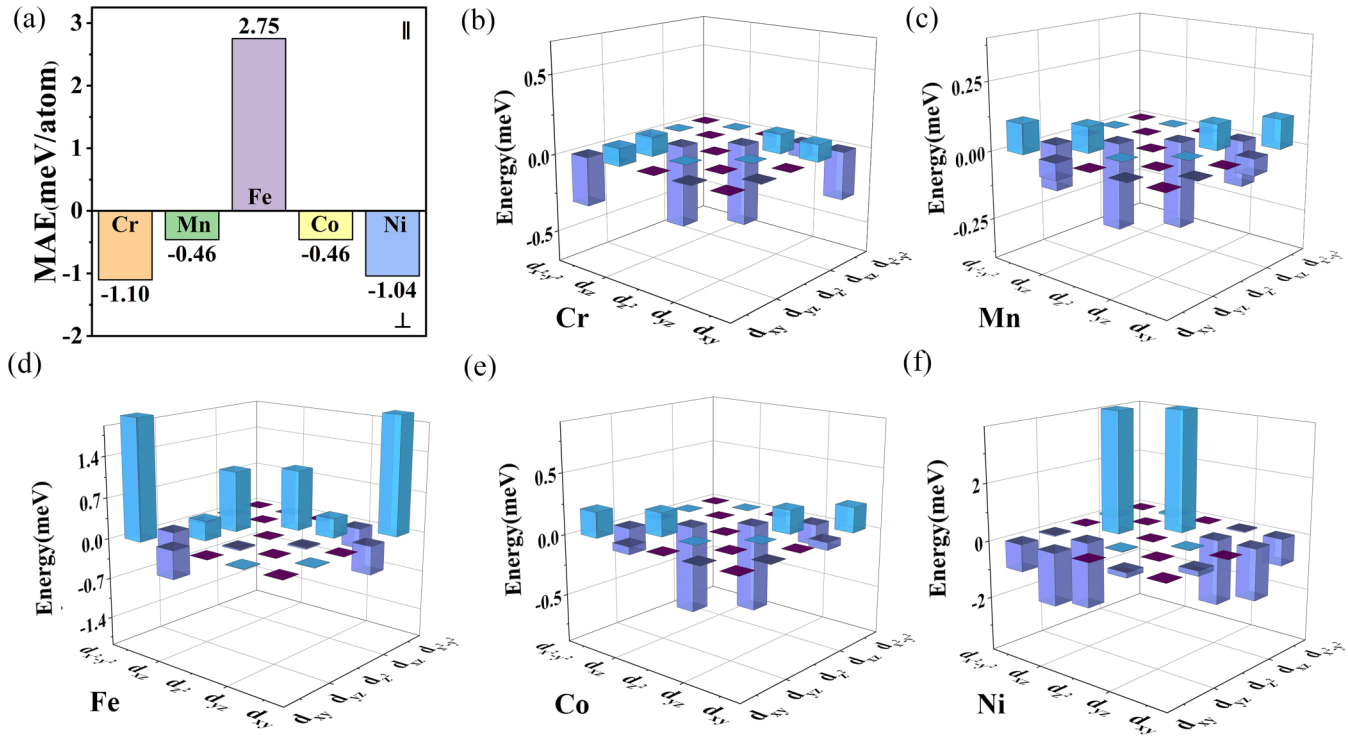

FIG. 6. (a) MAE of TMs-doped layer phases. Fe-doped layer phase is in-plane anisotropy, and Cr-, Mn-, Co-, and Ni-doped layer phases are out-of-plane anisotropy. (b)–(f) SOC matrix of TMs in layers. The column at the intersection of the straight line represents the energy change caused by the coupling of the two orbits. Column >0 meV represents in-plane anisotropy, and column <0 meV represents out-of-plane anisotropy.

theorem [36]:

$$\mathbf{MAE}(\boldsymbol{k}) = \sum_{k} \left[\boldsymbol{n}_i^{001} \boldsymbol{\varepsilon}_i^{001} - \boldsymbol{n}_{i'}^{100} \boldsymbol{\varepsilon}_{i'}^{100} \right], \tag{17}$$

where k and i are the k point and band indexes of the magnetization direction along [100] and [001], respectively, $\boldsymbol{n}_i$ is the occupation number of this band, and $\boldsymbol{\varepsilon}_i$ is the energy of band i at k point. The anisotropic energy of k point fluctuates in the two-dimensional Brillouin zone as shown in Figs. S7(a)–S7(e) [15]. In the Cr/Fe/Ni doped layer phase, the energy distribution tends to be close to zero near the $\boldsymbol{\Gamma}$ point, indicating that the eigenvalues at this point are not susceptible to the influence of the magnetic field [37]. Since the SOC interaction breaks the symmetry of the two-dimensional Brillouin zone, the energy eigenvalues of k points with respect to the symmetry of high symmetric points in k space are not equal. It is shown that the energy difference of the layered phase in different magnetization directions is large when it is near the boundary of the two-dimensional Brillouin zone.

We further analyze the contributions to MAE at atomic level, in order to gain the insight into the origin of the magnetic anisotropy. The matrix of SOC, containing the contribution from the hybridization between each of two d orbits of TM atoms, is calculated. According to the energy shown by the SOC matrix, most of the anisotropic energy comes from the coupling between d orbitals of TM atoms. This is mainly due to the fact that the valence electrons of other elements are p electrons and do not have strong anisotropy. The components are plotted as Figs. 6(b)–6(e). The expectation value of E_{soc} is twice the actual value of the total energy correction to the second order in SOC, i.e., $\mathbf{MAE} \approx \mathbf{0.5}\boldsymbol{\Delta E}_{\mathrm{soc}}$ [37]. Different matrix elements make different contributions to the orientation of anisotropy, and the overall easy magnetization orientation is determined by the summation of all of them. The overlapping matrixes for Cr, Mn, and Co dopants are similar, while the d_{xz} and d_{yz} orbits are semifilled and can contribute perpendicular anisotropic energy when coupling with other orbits, and SOC matrix elements $\langle d_{xy}|H_{\mathrm{SO}}|d_{xz}\rangle$ and $\langle d_{yz}|H_{\mathrm{SO}}|d_{z^2}\rangle$ dominate the MAE. For Ni dopant, although the in-plane anisotropic energy by $\langle d_{yz}|H_{\mathrm{SO}}|d_{z^2}\rangle$ is extremely large, the out-of-plane coupling of other three components, $\langle d_{xy}|H_{\mathrm{SO}}|d_{x^2-y^2}\rangle$, $\langle d_{yz}|H_{\mathrm{SO}}|d_{x^2-y^2}\rangle$, and $\langle d_{yz}|H_{\mathrm{SO}}|d_{xz}\rangle$, reversed this trend. For Fe dopant, the in-plane coupling of $\langle d_{xy}|H_{\mathrm{SO}}|d_{x^2-y^2}\rangle$ or $\langle d_{xz}|H_{\mathrm{SO}}|d_{z^2}\rangle$ make the greatest contribution, so the in-plane anisotropy can be formed. It is really interesting to find that $\langle d_{xy}|H_{\mathrm{SO}}|d_{x^2-y^2}\rangle$ and $\langle d_{xz}|H_{\mathrm{SO}}|d_{z^2}\rangle$ play a different role. Considering the electron occupation, we can achieve that different occupation of d states lead to different anisotropy directions. When the d_{xy} and $d_{x^2-y^2}$ are half-occupied, the anisotropy is the strongest tends to be in-plane anisotropy. On the basis of the half-occupied state, the increase or decrease of electrons would both weaken the in-plane anisotropy and even make it turn out-of-plane.

IV. CONCLUSIONS

In summary, we conducted a combined DFT and Monte Carlo study of magnetic ordering in both bulk and layer $Bi_{2-n}X_nO_2Se$ by a magnetic element doping scheme. It is found that all of the doping elements we used, Cr, Mn, Fe,

Co, and Ni, can induce very strong spin polarization, while the T_c of $Bi_{1.9375}Ni_{0.0625}O_2Se$ can be as high as 199 K. Particularly, their layered phase counterparts are investigated and the enhanced ferromagnetic properties are found, e.g., a T_c reaching to 317 K for layered $Bi_{1.75}Co_{0.25}O_2Se$. On the basis of these simulation results, we explore the origin of the magnetic order from the perspective of exchange mechanisms. Investigated bulk and layers phases were identified as ferromagnetic semiconductors with largest band gaps of 0.62 and 1.48 eV, respectively. We demonstrated that the robust long-range ferromagnetic ordering aligns in the in-plane direction of Fe-doped layer phase and in the out-of-plane direction of Cr-, Mn-, Co-, and Ni-doped layer phase, respectively. We analyze the origin of the out-of-plane MAE that is crucial for the 2D materials to have long-range order for finite temperatures. Our theoretical exploration provides guidance for the study of its properties, and motivates the further study of those systems with the aim to tailor their magnetic properties of doped layer Bi_2O_2Se for novel electronic applications.

ACKNOWLEDGMENTS

Q.F.Z. was supported by National Key Research and Development Program of China (No. 2017YFB0702100), National Natural Science Foundation of China (11404017), Technology Foundation for Selected Overseas Chinese Scholar, Ministry of Human Resources and Social Security of China, and Beijing Natural Science Foundation (2192029). D.L. acknowledges support by the European Regional Development Fund in the IT4Innovations national supercomputing center—path to Exascale project, project number CZ.02.1.01/0.0/0.0/16_013/0001791 within the Operational Programme Research, Development and Education, Grant No. 17-27790S of the Czech Science Foundations, and Mobility Project No. 8J18AT004 and SGS Grant No. SP2019/110. R.F.Z. was supported by the National Natural Science Foundation of China (NFSC) with No. 51672015, National Thousand Young Talents Program of China, and Fundamental Research Funds for the Central Universities.

[1] K. Sato, L. Bergqvist, J. Kudrnovský, P. H. Dederichs, O. Eriksson, I. Turek, B. Sanyal, G. Bouzerar, H. Katayama-Yoshida, V. A. Dinh, T. Fukushima, H. Kizaki, and R. Zeller, Rev. Mod. Phys. **82**, 1633 (2010).

[2] C. Freysoldt, B. Grabowski, T. Hickel, J. Neugebauer, G. Kresse, A. Janotti, and C. G. Van de Walle, Rev. Mod. Phys. **86**, 253 (2014).

[3] C. Gong, L. Li, Z. Li, H. Ji, A. Stern, Y. Xia, T. Cao, W. Bao, C. Wang, Y. Wang, Z. Q. Qiu, R. J. Cava, S. G. Louie, J. Xia, and X. Zhang, Nature (London) **546**, 265 (2017).

[4] B. Li, T. Xing, M. Zhong, L. Huang, N. Lei, J. Zhang, J. Li, and Z. Wei, Nat Commun **8**, 1958 (2017).

[5] Q. Pei, Y. Song, X. C. Wang, J. J. Zou, and W. B. Mi, Sci. Rep. **7**, 9504 (2017).

[6] N. D. Mermin and H. Wagner, Phys. Rev. Lett. **17**, 1133 (1966).

[7] M. Meng, S. Huang, C. Tan, J. Wu, Y. Jing, H. Peng, and H. Q. Xu, Nanoscale **10**, 2704 (2018).

[8] J. Wu, Y. Liu, Z. Tan, C. Tan, J. Yin, T. Li, T. Tu, and H. Peng, Adv. Mater. **29**, 1704060 (2017).

[9] J. Wu *et al.*, Nat. Nanotechnol. **12**, 530 (2017).

[10] Q. G. Li, X. Ma, and Z. Q. Kou, Phys. Rev. B **69**, 014409 (2004).

[11] Y. Fang, S. Wu, Z.-Z. Zhu, and G.-Y. Guo, Phys. Rev. B **98**, 125416 (2018).

[12] G. Kresse and J. Furthmüller, Phys. Rev. B **54**, 11169 (1996).

[13] S. L. Dudarev, G. A. Botton, S. Y. Savrasov, C. J. Humphreys, and A. P. Sutton, Phys. Rev. B **57**, 1505 (1998).

[14] M. D. Krcha and M. J. Janik, Langmuir **29**, 10120 (2013).

[15] See Supplemental Material at http://link.aps.org/supplemental/10.1103/PhysRevB.100.054438 for Table S1, Figs. S1–S7, and supplementary notes about formation energy and electronic properties.

[16] J. Bai, J. M. Raulot, Y. D. Zhang, C. Esling, X. Zhao, and L. Zuo, J. Appl. Phys. **108**, 064904 (2010).

[17] D. Legut and J. Pavlu, J. Phys. Condens. Matter **24**, 195502 (2012).

[18] S. Maintz, V. L. Deringer, A. L. Tchougreeff, and R. Dronskowski, J. Comput. Chem. **34**, 2557 (2013).

[19] Y. Sun, W. Tong, X. J. Xu, and Y. H. Zhang, Phys. Rev. B **63**, 174438 (2001).

[20] S. J. Gilliland, J. A. Sans, J. F. Sánchez-Royo, G. Almonacid, B. García-Domene, A. Segura, G. Tobias, and E. Canadell, Phys. Rev. B **86**, 155203 (2012).

[21] K. Sato, W. Schweika, P. H. Dederichs, and H. Katayama-Yoshida, Phys. Rev. B **70**, 201202(R) (2004).

[22] S. Maintz, V. L. Deringer, A. L. Tchougreeff, and R. Dronskowski, J. Comput. Chem. **37**, 1030 (2016).

[23] V. L. Deringer, A. L. Tchougreeff, and R. Dronskowski, J. Phys. Chem. A **115**, 5461 (2011).

[24] S. Mi, S. H. Yuan, and P. Lyu, J. Appl. Phys. **109**, 083931 (2011).

[25] C. H. Ziener, S. Glutsch, and F. Bechstedt, Phys. Rev. B **70**, 075205 (2004).

[26] R. F. Evans, W. J. Fan, P. Chureemart, T. A. Ostler, M. O. Ellis, and R. W. Chantrell, J. Phys. Condens. Matter **26**, 103202 (2014).

[27] L. M. Sandratskii, E. Sasioglu, and P. Bruno, Phys. Rev. B **73**, 014430 (2006).

[28] J. P. Clancy, A. Lupascu, H. Gretarsson, Z. Islam, Y. F. Hu, D. Casa, C. S. Nelson, S. C. LaMarra, G. Cao, and Y. J. Kim, Phys. Rev. B **89**, 054409 (2014).

[29] A. Ramasubramaniam and D. Naveh, Phys. Rev. B **87**, 195201 (2013).

[30] N. Miao, B. Xu, L. Zhu, J. Zhou, and Z. Sun, J. Am. Chem. Soc. **140**, 2417 (2018).

[31] L. Chen, X. Yang, F. H. Yang, J. H. Zhao, J. Misuraca, P. Xiong, and S. von Molnar, Nano Lett. **11**, 2584 (2011).

[32] P. V. Balachandran, D. Z. Xue, and T. Lookman, Phys. Rev. B **93**, 144111 (2016).

[33] J.-M. Zhang, W. Ming, Z. Huang, G.-B. Liu, X. Kou, Y. Fan, K. L. Wang, and Y. Yao, Phys. Rev. B **88**, 235131 (2013).

[34] H. X. Yang, M. Chshiev, B. Dieny, J. H. Lee, A. Manchon, and K. H. Shin, Phys. Rev. B **84**, 054401 (2011).

[35] J. C. Leiner, T. Kim, K. Park, J. Oh, T. G. Perring, H. C. Walker, X. Xu, Y. Wang, S.-W. Cheong, and J. G. Park, Phys. Rev. B **98**, 134412 (2018).

[36] M. Weinert, R. E. Watson, and J. W. Davenport, Phys. Rev. B **32**, 2115 (1985).

[37] J. Qiao, S. Peng, Y. Zhang, H. Yang, and W. Zhao, Phys. Rev. B **97**, 054420 (2018).